Astronomy & Astrophysics manuscript no. paper
December 29, 2020

Time delay estimation in unresolved lensed quasars

Author1[1] and Author2[2,⋆]

[1] Institute for Astronomy (IfA), University of Vienna, Türkenschanzstrasse 17, A-1180 Vienna
e-mail: wuchterl@amok.ast.univie.ac.at
[2] University of Alexandria, Department of Geography, ...
e-mail: c.ptolemy@hipparch.uheaven.space ⋆⋆

Received September 15, 1996; accepted March 16, 1997

ABSTRACT

Context. Early universe (EU) measurements and late universe (LU) observations have resulted in a tension on the estimated value of the Hubble parameter H_0. Time-delay cosmography offers an alternative method to measure H_0. In this respect, the H0LiCoW collaboration has reported a 2.4% measurement of H_0 compatible with LU observations, increasing the tension at the 5.3σ level. Whereas, TDCOSMO+SLACS has reported a 5% measurement of H_0 in agreement with both EU and LU estimates, showing the need to collect more data in order to reduce the uncertainty in the H_0 estimation.
Aims. In time-delay cosmography, the fractional uncertainty on H_0 is directly related to the uncertainty on relative time delays measurements and it linearly decreases with the number of lensed systems considered. Therefore, in order to reduce it, more lensed systems should be analysed and, possibly, with a regular and long-term monitoring, of the order of years. This cannot be achieved with big telescopes, due to the huge amount of observational requests they have to fulfill. On the other hand, small/medium-sized telescopes are present in a much larger number and are often characterized by more versatile observational programs. However, the limited resolution capabilities of such instruments and their often not privileged geographical location may prevent them from providing well-separated images of the same lensed source.
In this work, we present a novel approach to estimate the time-delay in unresolved lensed quasar systems. Our proposal is further motivated by recent developments in discovering more unresolved strongly-lensed QSO systems.
Methods. Our method uses ...
Results. ...

Key words. Gravitational lensing – Hubble parameter – Quasars – Galaxies – Machine Learning

1. Introduction

The Hubble parameter H_0 quantifies the current expansion rate of the Universe. The measured values of H_0 from different observations led to a tension. In particular, EU observations [Aghanim et al. (2020)] have measured $H_0 = 67.4 \pm 0.5$ km s^{-1} Mpc^{-1}, whereas, LU observations [Riess et al. (2019)] give $H_0 = 74.03 \pm 1.42$ km s^{-1} Mpc^{-1}, resulting in a tension of about 4.4σ.
As first pointed out in [Refsdal (1964)], time-delay cosmography offers an alternative way of determining the Hubble parameter: the light rays coming from a distant source, e.g. a quasar, can be deflected by the gravitational field of an intervening massive object, e.g. a galaxy. If the field is strong enough, multiple images of the same source are observed and, by tracking the light intensity of each image over time, a *light curve* is obtained. Light curves associated with different images will exhibit a mutual time-delay (ΔT), due to the different paths that the photons have travelled. As shown in [Refsdal (1964)], this time-delay is related to the Hubble parameter as $H_0 \propto 1/\Delta T$. The major results obtained via time-delay cosmography come from the H0LiCOW collaboration [Wong et al. (2020)], who found $H_0 = 73.3^{+1.7}_{-1.8}$ km s^{-1} Mpc^{-1} from a sample of six lensed quasars monitored by the COSMOGRAIL project [Millon et al. (2020)], enhancing the tension up to 5.3σ. However, a more recent analysis of 40 strong gravitational lenses, from TDCOSMO+SLACS [Birrer et al. (2020)], found $H_0 = 67.4^{+4.1}_{-3.2}$ km s^{-1} Mpc^{-1}, relaxing the Hubble tension and demonstrating the importance of understanding the lenses mass density profiles. This scenario motivates further studies aimed at improving the precision in the H_0 estimation.
In this respect, the fractional error of H_0, for an ensemble of N Gravitationally Lensed Quasars (GLQs), is related to the uncertainties in the time-delay estimation $\sigma_{\Delta T}$, line-of-sight convergence σ_{los} and lens surface density $\sigma_{\langle k \rangle}$ as [Tie & Kochanek (2017)]:

$$\frac{\sigma_H^2}{H_0^2} \sim \frac{\sigma_{\Delta T}^2/\Delta T^2 + \sigma_{los}^2 + \sigma_{\langle k \rangle}^2}{N} \tag{1}$$

where the first two terms are dominated by random errors and their contribution to the overall error scales as $N^{-1/2}$. Therefore, increasing the sample of analysed GLQs allows to reduce the error on H_0.
In this paper we focus on the time delay estimation and its relative error.
To date, a sample of about 220 GLQs is available[1]. However, only a very small subset, with well separated multiple images, has been used to measure H_0. The reason is that it is easier and safer to extract information from such systems, and consequently reduce the error on H_0.

⋆ Just to show the usage of the elements in the author field
⋆⋆ The university of heaven temporarily does not accept e-mails

[1] https://research.ast.cam.ac.uk/lensedquasars/index.html

In this respect, Fig. 1 (bottom) shows the magnitude of the multiple images versus the maximum image separation for the known GLQs. Systems being part of the grey region, which represent 70% of the total sample (as shown in the up-right histogram), have a maximum image separation below 2 arcsec.

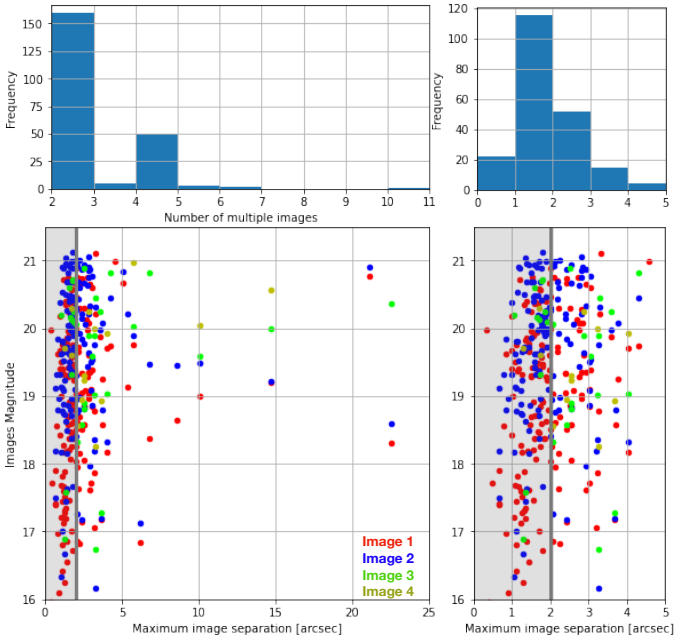

Fig. 1. Top-left: distribution of known GLQs as a function of the number of multiple images. Top-right: distribution of known GLQs as a function of the maximum image separation. Bottom (left and right): Magnitude of the multiple images versus the maximum image separation. The grey region contains 70% of the total GLQ sample.

In addition, [Shu et al. (2020)] presented a new method to find GLQs from unresolved light curves. Such systems have therefore even smaller separation between multiple images.
This would make big telescopes the ideal instruments to perform lensed quasars monitoring, both in light of their high angular resolution and the geographical areas they are placed in, where the effects of atmospheric turbulence are less prominent. However, because of the time scales of the intrinsic variations of the sources, such observation campaigns should last years [Millon et al. (2020)]. Therefore, due to the amount of observational requests that big telescopes have to fulfil, they hardly can be employed for these purposes. On the other hand, small/medium sized telescopes (1-2m) [Borgeest et al. (1996)] can be used. Unfortunately, their already reduced angular resolution is further worsened by their often less privileged geographical positions, in terms of atmospheric seeing, which can reach 3 arcsec [Karttunen (2016)].
Therefore, the majority of GLQs already known, together with future discoveries, will mainly appear as a single image for small/medium-size telescopes. For this reason, here we propose a novel approach, based on Machine Learning (ML) algorithms, to estimate the time-delay from unresolved GLQ light curves.
For simplicity, in this work we focus on double-lensed GLQs. This choice is further motivated by the fact that the majority of the already known systems are doubles, as shown in Fig. 1 (top-left). However, [Shu et al. (2020)] expect to find a consistent quantity of quadruply-imaged QSOs in the future. Therefore, we plan to extend our work for systems with N>2 images.
The paper is structured as follows: Sec. 2 describes the ML-based method we use for evaluating the time delay between multiple images. Sec. 3 describes the Monte Carlo (MC) simulations needed to train our ML algorithm. Sec. 4 shows the results of our method in a test dataset obtained by simulating the real systems RXJ1131. Finally, Sec. 5 shows our evaluated time delays for real systems and compare it with other estimations.

2. Time delay estimation with ML technique

3. Light Curves Simulation

4. Test approach on fake dataset

5. Results on real data

params

M_r	mass internal to the radius r
m	mass of the zone
r_0	unperturbed zone radius
ρ_0	unperturbed density in the zone
T_0	unperturbed temperature in the zone
L_{r0}	unperturbed luminosity
$E_{\rm th}$	thermal energy of the zone

and with the definitions of the *local cooling time* (see Fig. 2)

$$\tau_{\rm co} = \frac{E_{\rm th}}{L_{r0}}, \tag{2}$$

and the *local free-fall time*

$$\tau_{\rm ff} = \sqrt{\frac{3\pi}{32G}\frac{4\pi r_0^3}{3M_{\rm r}}}, \tag{3}$$

Baker's K and σ_0 have the following form:

$$\sigma_0 = \frac{\pi}{\sqrt{8}}\frac{1}{\tau_{\rm ff}} \tag{4}$$

$$K = \frac{\sqrt{32}}{\pi}\frac{1}{\delta}\frac{\tau_{\rm ff}}{\tau_{\rm co}}; \tag{5}$$

where $E_{\rm th} \approx m(P_0/\rho_0)$ has been used and

$$\delta = -\left(\frac{\partial \ln\rho}{\partial \ln T}\right)_P \qquad e = mc^2 \tag{6}$$

is a thermodynamical quantity which is of order 1 and equal to 1 for nonreacting mixtures of classical perfect gases. The physical meaning of σ_0 and K is clearly visible in the equations above. σ_0 represents a frequency of the order one per free-fall time. K is proportional to the ratio of the free-fall time and the cooling time. Substituting into Baker's criteria, using thermodynamic identities and definitions of thermodynamic quantities,

$$\Gamma_1 = \left(\frac{\partial \ln P}{\partial \ln\rho}\right)_S, \ \chi_\rho = \left(\frac{\partial \ln P}{\partial \ln\rho}\right)_T, \ \kappa_P = \left(\frac{\partial \ln\kappa}{\partial \ln P}\right)_T$$

$$\nabla_{\rm ad} = \left(\frac{\partial \ln T}{\partial \ln P}\right)_S, \ \chi_T = \left(\frac{\partial \ln P}{\partial \ln T}\right)_\rho, \ \kappa_T = \left(\frac{\partial \ln\kappa}{\partial \ln T}\right)_T$$

one obtains, after some pages of algebra, the conditions for *stability* given below:

$$\frac{\pi^2}{8}\frac{1}{\tau_{\rm ff}^2}(3\Gamma_1 - 4) > 0 \tag{7}$$

$$\frac{\pi^2}{\tau_{\rm co}\tau_{\rm ff}^2}\Gamma_1\nabla_{\rm ad}\left[\frac{1-3/4\chi_\rho}{\chi_T}(\kappa_T - 4) + \kappa_P + 1\right] > 0 \tag{8}$$

$$\frac{\pi^2}{4}\frac{3}{\tau_{\rm co}\tau_{\rm ff}^2}\Gamma_1^2\nabla_{\rm ad}\left[4\nabla_{\rm ad} - (\nabla_{\rm ad}\kappa_T + \kappa_P) - \frac{4}{3\Gamma_1}\right] > 0 \tag{9}$$

Fig. 2. Adiabatic exponent Γ_1. Γ_1 is plotted as a function of lg internal energy [erg g^{-1}] and lg density [g cm^{-3}].

Table 1. Opacity sources.

Source	T/[K]
Yorke 1979, Yorke 1980a	≤ 1700[a]
Krügel 1971	$1700 \leq T \leq 5000$
Cox & Stewart 1969	$5000 \leq$

For a physical discussion of the stability criteria see **?** or **?**.

We observe that these criteria for dynamical, secular and vibrational stability, respectively, can be factorized into

1. a factor containing local timescales only,
2. a factor containing only constitutive relations and their derivatives.

The first factors, depending on only timescales, are positive by definition. The signs of the left hand sides of the inequalities (7), (8) and (9) therefore depend exclusively on the second factors containing the constitutive relations. Since they depend only on state variables, the stability criteria themselves are *functions of the thermodynamic state in the local zone*. The one-zone stability can therefore be determined from a simple equation of state, given for example, as a function of density and temperature. Once the microphysics, i.e. the thermodynamics and opacities (see Table 1), are specified (in practice by specifying a chemical composition) the one-zone stability can be inferred if the thermodynamic state is specified. The zone – or in other words the layer – will be stable or unstable in whatever object it is imbedded as long as it satisfies the one-zone-model assumptions. Only the specific growth rates (depending upon the time scales) will be different for layers in different objects.

We will now write down the sign (and therefore stability) determining parts of the left-hand sides of the inequalities (7), (8) and (9) and thereby obtain *stability equations of state*.

The sign determining part of inequality (7) is $3\Gamma_1 - 4$ and it reduces to the criterion for dynamical stability

$$\Gamma_1 > \frac{4}{3}\cdot \tag{10}$$

Stability of the thermodynamical equilibrium demands

$$\chi_\rho > 0, \quad c_v > 0\,, \tag{11}$$

and

$$\chi_T > 0 \tag{12}$$

holds for a wide range of physical situations. With

$$\Gamma_3 - 1 = \frac{P}{\rho T}\frac{\chi_T}{c_v} \quad > \quad 0 \tag{13}$$

$$\Gamma_1 = \chi_\rho + \chi_T(\Gamma_3 - 1) \quad > \quad 0 \tag{14}$$

$$\nabla_{\rm ad} = \frac{\Gamma_3 - 1}{\Gamma_1} \quad > \quad 0 \tag{15}$$

Fig. 3. Vibrational stability equation of state $S_{\rm vib}(\lg e, \lg \rho)$. > 0 means vibrational stability.

we find the sign determining terms in inequalities (8) and (9) respectively and obtain the following form of the criteria for dynamical, secular and vibrational *stability*, respectively:

$$3\Gamma_1 - 4 =: S_{\rm dyn} > \quad 0 \tag{16}$$

$$\frac{1 - 3/4\chi_\rho}{\chi_T}(\kappa_T - 4) + \kappa_P + 1 =: S_{\rm sec} > \quad 0 \tag{17}$$

$$4\nabla_{\rm ad} - (\nabla_{\rm ad}\kappa_T + \kappa_P) - \frac{4}{3\Gamma_1} =: S_{\rm vib} > \quad 0\,. \tag{18}$$

The constitutive relations are to be evaluated for the unperturbed thermodynamic state (say (ρ_0, T_0)) of the zone. We see that the one-zone stability of the layer depends only on the constitutive relations Γ_1, $\nabla_{\rm ad}$, χ_T, χ_ρ, κ_P, κ_T. These depend only on the unperturbed thermodynamical state of the layer. Therefore the above relations define the one-zone-stability equations of state $S_{\rm dyn}$, $S_{\rm sec}$ and $S_{\rm vib}$. See Fig. 3 for a picture of $S_{\rm vib}$. Regions of secular instability are listed in Table 1.

6. Conclusions

1. The conditions for the stability of static, radiative layers in gas spheres, as described by Baker's (**?**) standard one-zone model, can be expressed as stability equations of state. These stability equations of state depend only on the local thermodynamic state of the layer.
2. If the constitutive relations – equations of state and Rosseland mean opacities – are specified, the stability equations of state can be evaluated without specifying properties of the layer.
3. For solar composition gas the κ-mechanism is working in the regions of the ice and dust features in the opacities, the H_2 dissociation and the combined H, first He ionization zone, as indicated by vibrational instability. These regions of instability are much larger in extent and degree of instability than the second He ionization zone that drives the Cepheïd pulsations.

Acknowledgements. Part of this work was supported by the German *Deutsche Forschungsgemeinschaft, DFG* project number Ts 17/2–1.

References

Aghanim, N., Akrami, Y., Ashdown, M., et al. 2020, Astronomy & Astrophysics, 641, A6
Birrer, S., Shajib, A. J., Galan, A., et al. 2020, Astronomy & Astrophysics, 643, A165
Borgeest, U., Schramm, K.-J., & Von Linde, J. 1996, in Examining Big Bang Diffus. Backgr. Radiations (Springer Netherlands), 527–528
Karttunen, H. 2016, Fundamental astronomy (Heidelberg: Springer)
Millon, M., Courbin, F., Bonvin, V., et al. 2020, Astron. Astrophys. [arXiv:2002.05736]
Refsdal, S. 1964, Monthly Notices of the Royal Astronomical Society, 128, 307
Riess, A. G., Casertano, S., Yuan, W., Macri, L. M., & Scolnic, D. 2019, The Astrophysical Journal, 876, 85
Shu, Y., Belokurov, V., & Evans, N. W. 2020, Discovering Strongly-lensed QSOs From Unresolved Light Curves
Tie, S. S. & Kochanek, C. S. 2017, Monthly Notices of the Royal Astronomical Society, 473, 80–90
Wong, K. C., Suyu, S. H., Chen, G. C.-F., et al. 2020, Mon. Not. R. Astron. Soc. [arXiv:arXiv:1907.04869v2]